Graphene plasmonics for tuning photon decay rate near metallic split-ring resonator in a multilayered substrate

Yongpin P. Chen,[1,2] **Wei E. I. Sha,**[2] **Lijun Jiang,**[2,*] **and Jun Hu**[1]

[1] *School of Electronic Engineering, University of Electronic Science and Technology of China,*
Chengdu, 611731, China
[2] *Department of Electrical and Electronic Engineering, The University of Hong Kong,*
Pokfulam, Hong Kong, China
[*] *jianglj@hku.hk*

Abstract: Study of photon decay rate is essential to various optical devices, where graphene is an emerging building block due to its electrical tunability. In this paper, we study photon decay rate of a quantum emitter near a metallic split-ring resonator, which is embedded in a multilayered substrate incorporating a graphene layer. Analyzing photon decay rate in such a complex multilayered system is not only computationally challenging but also highly important to experimentally realizable devices. First, the dispersion relation of graphene plasmonics supported at a dieletric/graphene/dielectric structure is investigated systematically. Meanwhile, the dispersion relation of metallic plasmonics supported at a dielectric/metal structure is studied comparatively. According to our investigation, graphene offers several flexible tuning routes for manipulating photon decay rate, including tunable chemical potential and the emitter's position and polarization. Next, considering plasmonic waves in a graphene sheet occur in the infrared regime, we carefully design a metallic split ring resonating around the same frequency range. Consequently, this design enables a mutual interaction between graphene plasmonics and metallic plasmonics. The boundary element method with a multilayered medium Green's function is adopted in the numerical simulation. Blue-shifted and splitting resonance peaks are theoretically observed, which suggests a strong mode coupling. Moreover, the mode coupling has a switch on-off feature via electrostatically doping the graphene sheet. This work is helpful to dynamically manipulate photon decay rate in complex optical devices.

OCIS codes: (050.1755) Computational electromagnetic methods; (250.5403) Plasmonics; (230.4555) Coupled resonators.

References and links

1. A. Kinkhabwala, Z. Yu, S. Fan, Y. Avlasevich, K. Müllen, and W. E. Moerner, "Large single-molecule fluorescence enhancements produced by a bowtie nanoantenna," Nat. Photon. **3**, 654–657 (2009).
2. K. G. Lee, X. W. Chen, H. Eghlidi, P. Kukura, R. Lettow, A. Renn, V. Sandoghdar, and S. Götzinger, "A planar dielectric antenna for directional single-photon emission and near-unity collection efficiency," Nat. Photon. **5**(3), 166–169 (2011).
3. X. W. Chen, M. Agio, and V. Sandoghdar, "Metallodielectric hybrid antennas for ultrastrong enhancement of spontaneous emission," Phys. Rev. Lett. **108**(23), 233001 (2012).

#225356 - $15.00 USD Received 21 Oct 2014; revised 19 Dec 2014; accepted 19 Dec 2014; published 30 Jan 2015

4. J. Vučković, M. Lončar, and A. Scherer, “Surface plasmon enhanced light-emitting diode,” IEEE J. Quantum Electron. **36**(10), 1131–1144 (2000).
5. C. Walther, G. Scalari, M. I. Amanti, M. Beck, and J. Faist, “Microcavity laser oscillating in a circuit-based resonator,” Science **327**, 1495–1497 (2010).
6. J. Goffard, D. Gérard, P. Miska, A.-L. Baudrion, R. Deturche, and J. Plain, “Plasmonic engineering of spontaneous emission from silicon nanocrystals,” Sci. Rep. **3**, 2672 (2013).
7. L. Novotny and B. Hecht, *Principles of Nano-optics* (Cambridge University, 2006).
8. M. Paulus, P. Gay-Balmaz, and O. J. F. Martin, “Accurate and efficient computation of the Green’s tensor for stratified media,” Phys. Rev. E **62**(4), 5797–5807 (2000).
9. A. M. Kern and O. J. F. Martin, “Surface integral formulation for 3D simulations of plasmonic and high permittivity nanostructures,” J. Opt. Soc. Am. A **26**(4), 732–740 (2009).
10. E. Simsek, Q. H. Liu, and B. Wei, “Singularity subtraction for evaluation of Green’s functions for multilayer media,” IEEE Trans. Micro. Theory Tech. **54**(1), 216–225 (2006).
11. E. Simsek, “Graphene in layered medium applications,” Micro. Opt. Tech. Lett. **55**(10), 2293–2296 (2013).
12. Y. P. Chen, W. C. Chew, and L. Jiang, “A new Green’s function formulation for modeling homogeneous objects in layered medium,” IEEE Trans. Antennas Propag. **60**(10), 4766–4776 (2012).
13. Y. P. Chen, W. E. I. Sha, W. C. H. Choy, L. Jiang, and W. C. Chew, “Study on spontaneous emission in complex multilayered plasmonic system via surface integral equation approach with layered medium Green’s function,” Opt. Express **20**(18), 20210–20221 (2012).
14. K. J. Russell, T.-L. Liu, S. Cui, and E. L. Hu, “Large spontaneous emission enhancement in plasmonic nanocavities,” Nat. Photo. **6**, 459–462 (2012).
15. Ekmel Ozbay, “Plasmonics: merging photonics and electronics at nanoscale dimensions,” Science **311**, 189–193 (2006).
16. A. K. Geim and K. S. Novoselov, “The rise of graphene,” Nat. Mater. **6**, 183–191 (2007).
17. M. Jablan, H. Buljan, and M. Soljačić, “Plasmonics in graphene at infrared frequencies,” Phys. Rev. B **80**, 245435 (2009).
18. F. J. García de Abajo, “Graphene plasmonics: challenges and opportunities,” ACS Photo. **1**(3), 135–152 (2014).
19. T. Low and P. Avouris, ”Graphene plasmonics for terahertz to mid-infrared applications,” ACS Nano **8**(2), 1086–1101 (2014).
20. G. W. Hanson, “Dyadic Green’s functions and guided surface waves for a surface conductivity model of graphene,” J. Appl. Phys. **103**, 064302 (2008).
21. M. Engel, M. Steiner, A. Lombardo, A. C. Ferrari, H. v. Löhneysen, P. Avouris, and R. Krupke, “Light-matter interaction in a microcavity-controlled graphene transistor” Nat. Comm. **3**, 906 (2012).
22. F. H. L. Koppens, D. E. Chang, and F. J. García de Abajo, “Graphene plasmonics: a platform for strong light-matter interactions,” Nano Lett. **11**(8), 3370–3377 (2011).
23. H. Yan, F. Xia, Z. Li, and P. Avouris, “Plasmonics of coupled graphene micro-structures,” New J. Phys. **14**, 125001 (2012).
24. A. Kumar, K. H. Fung, M. T. H. Reid, and N. X. Fang, “Photon emission rate engineering using graphene nanodisc cavities,” Opt. Express **22**(6), 6400–6415 (2014).
25. Y. Yao, M. A. Kats, P. Genevet, N. Yu, Y. Song, J. Kong, and F. Capasso, “Broad electrical tuning of graphene-loaded plasmonic antennas,” Nano Lett. **13**(3), 1257–1264 (2013).
26. A. Mock, “Padé approximant spectral fit for FDTD simulation of graphene in the near infrared,” Opt. Mater. Express **2**(6), 771–781 (2012).
27. W. C. Chew, *Waves and Fields in Inhomogeneous Media* (Van Nostrand Reinhold, 1990).
28. S. A. Maier, *Plasmonics: Fundamentals and Applications* (Springer Science+Business Media LLC, 2007).
29. A. D. Rakic, A. B. Djurisic, J. M. Elazar, and M. L. Majewski, “Optical properties of metallic films for vertical-cavity optoelectronic devices,” Appl. Opt. **37**(22), 5271–5283 (1998).

---

1. Introduction

Study of photon decay rate in a multilayered system with complicated metallic nano-scatterers plays an important role in the design of various optical and optoelectronic devices, such as optical antennas, light-emitting diodes, lasers, solar cells, etc [1–6]. On one hand, due to the fabrication technology, most functional devices have a layered structure. Simulations should model the layered structure accurately in order to achieve a good theoretical perdition. On the other hand, photon decay rate is determined by the interaction between the emitter and its local electromagnetic environment. By manipulating local density of states (LDOS), the photon decay rate can be well controlled. LDOS counts the number of electromagnetic modes at the emitter point. Each electromagnetic mode can be taken as a decay channel. The more decay channels there are, the easier it is for an excited atom emits photons via returning to its ground state. Based on the eigen-mode expansion, the LDOS can be expressed in terms of the imaginary part of the dyadic Green's function [7]. Therefore, determining the photon decay rate is equivalent to the calculation of the Green's tensor in a complex electromagnetic environment. Considering the multilayered substrate and the complex structure embedded in it, the boundary element method with the kernel of a multilayered medium Green's function [8–13] is a favorable choice for the numerical simulation.

Plasmonic effects of metals in the visible light regime have been employed to control the photon decay rate in designs of various optical and optoelectronic devices [14, 15]. However, metals suffer from several drawbacks to manipulate photon decay rate, such as a large Ohmic loss in the frequency regime of interest and limited dynamic tunability of carrier density. Recently, graphene has become an alternative plasmonic material with several extraordinary properties [16–19]. Graphene is a two-dimensional (2D) sheet of carbon atoms bonded in a honeycomb lattice. Due to a unique energy-momentum relationship, electrons in graphene behave like Dirac fermions [20]. As a result, graphene plasmons are much less lossy in the far infrared or terahertz regime compared to metals in the visible light regime. What is more, graphene can be doped to a high carrier concentration by electrostatic gating and chemical doping. Consequently, graphene is an excellent candidate to engineer the photon decay rate. Besides, considering a fast progress in experimental tools, the ultrathin graphene layer can be easily integrated with a layered substrate [21].

The influence of graphene plasmonics on the photon decay rate has received much attention recently [22–24]. However, most of the research works consider a single graphene sheet or graphene attached to a simple substrate. Regarding the coupling and hybridization effects between a graphene layer and complicated metallic nanostructures, few works have been done until now. It is interesting to study the coupling between metallic plasmonics and graphene plasmonics; and simultaneously their effects on the photon decay rate. In view of a distinct working frequency gap between graphene plasmonics and metallic plasmonics, a physical realization of their coupling is fairly difficult. Here we carefully design a metallic split-ring resonator, which resonates in the same frequency band of the electrostatically doped graphene. The resonator is integrated in a practical multilayered substrate involving a graphene layer. The photon decay rate can therefore be manipulated by the external gate voltage, as well as the position and polarization of the quantum emitter. Such tunable properties are favorable in the design of functional devices.

In this paper, we will first briefly review the methodology used in the simulation, namely the boundary element method with the kernel of a multilayered medium Green's function. Second, the dispersion relation of graphene plasmonics and metallic plasmonics are comparatively investigated, revealing distinguished features of photon decay rates with respect to their working frequency regimes. Finally, the mode coupling of the graphene and a split-ring resonator integrated in a layered substrate is studied. It is found that by increasing chemical potential, the resonance peak of the hybrid system is blue-shifted [25] and splits.

2. Methodology

The photon decay rate in an inhomogeneous environment is calculated by the imaginary part of the dyadic Green's function evaluated at the location of the emitter [7]:

$$\frac{\gamma}{\gamma_0} = \frac{\operatorname{Im}\left[G_{\alpha\alpha}(\mathbf{r},\mathbf{r},\omega)\right]}{\operatorname{Im}\left[G_{0\alpha\alpha}(\mathbf{r},\mathbf{r},\omega)\right]} \tag{1}$$

where $G_{\alpha\alpha}$ is the diagonal entries of the dyadic Green's function with $\alpha = x, y, z$, and the quantity with subscript 0 denotes the counterpart in the referenced homogeneous background.

#225356 - $15.00 USD Received 21 Oct 2014; revised 19 Dec 2014; accepted 19 Dec 2014; published 30 Jan 2015

In principle, getting the Green's function is equivalent to finding the total electric field generated by a Hertzian dipole in such an inhomogeneous environment:

$$E_\alpha(\mathbf{r}) = -j\omega\mu \int_V G_{\alpha\alpha}(\mathbf{r},\mathbf{r}')\delta(\mathbf{r}-\mathbf{r}')d\mathbf{r}' \tag{2}$$

where the time convention $e^{j\omega t}$ is assumed and suppressed. According to this definition, $\mathrm{Im}(G_{\alpha\alpha})$ is translated to $\mathrm{Re}(E_\alpha)$. Hence, this problem can be cast to a classical electromagnetic radiation/scattering problem.

We investigate the schematic configuration as shown in Fig. 1, where a complex metallic split-ring resonator is embedded in a multilayered structure incorporating a graphene layer.

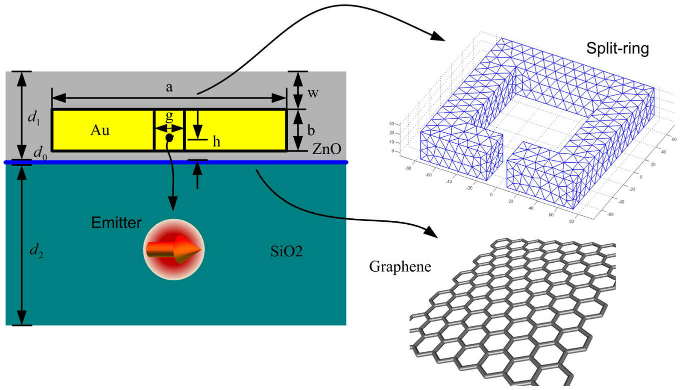

Fig. 1. The schematic configuration of a complicated electromagnetic system for manipulating photon decay rates. A rectangular gold (Au) split-ring resonator is embedded in the layer of ZnO with thickness $d_1 = 60$ nm and dielectric constant (relative permittivity) $\varepsilon_{1r} = 3.61$. The ZnO layer is attached to a graphene layer, which is backed by a SiO_2 substrate with $d_2 = 100$ nm and $\varepsilon_{2r} = 2.25$. The mesh of the resonator is shown in the figure with $a = 150$ nm, $b = 30$ nm, $g = 20$ nm, and $w = 25$ nm. The emitter is put inside the gap of this resonator. The effective thickness of the graphene layer is set to be a typical value of $d_0 = 0.5$ nm.

The excitation of this system is a quantum emitter modeled by an electric Hertzian dipole. To calculate the electric field or Green's function at the source location, the boundary element method in computational electromagnetics is a favorable choice. Considering the multilayered substrate including the graphene layer, we further incorporate the multilayered medium Green's function as the integration kernel to simplify the numerical modeling. The detailed mathematical expressions and implementation procedure can be found in [12,13] and will not be repeated here.

It is worthy of mentioning that graphene is usually defined as an infinitely thin material with a surface conductivity. This conductivity can be calculated by Kubo formula as a function of frequency (ω), chemical potential (μ_c), carrier scattering rate (Γ), and temperature (T): [20,26]

$$\begin{aligned} \sigma(\omega,\mu_c,\Gamma,T) \quad &= \frac{je^2(\omega-j2\Gamma)}{\pi\hbar^2}\left[\frac{1}{(\omega-j2\Gamma)^2}\int_0^\infty \varepsilon\left(\frac{\partial f_d(\varepsilon)}{\partial\varepsilon}-\frac{\partial f_d(-\varepsilon)}{\partial\varepsilon}\right)d\varepsilon\right. \\ &\left. -\int_0^\infty \frac{f_d(-\varepsilon)-f_d(\varepsilon)}{(\omega-j2\Gamma)^2-4(\varepsilon/\hbar)^2}d\varepsilon\right]. \end{aligned} \tag{3}$$

where $\hbar$ is the reduced Plank's constant, $f_d(\varepsilon) = \left(e^{(\varepsilon-\mu_c)/k_BT}+1\right)^{-1}$ is the Fermi-Dirac distribution, and k_B is the Boltzmann's constant. However, this 2D model is not consistent with

#225356 - $15.00 USD Received 21 Oct 2014; revised 19 Dec 2014; accepted 19 Dec 2014; published 30 Jan 2015

a general multilayered medium and the standard definition of reflection and transmission coefficients therein [27]. An alternative way is to define a there-dimensional (3D) model with a finite thickness and an effective volume conductivity $\widetilde{\sigma} = \sigma / d_0$, where d_0 is the effective thickness of the graphene sheet and a typical value of $d_0 = 0.5$ nm is adopted in this work. Hence, the effective dielectric constant of the graphene can be defined in the normal way as $\varepsilon_r(\omega) = 1 - j\widetilde{\sigma}/\omega\varepsilon_0$. In the following numerical experiments, if not otherwise specified, the default parameters for the graphene are: the chemical potential $\mu_c = 0.7$ eV, the temperature with room temperature $T = 300$ K, and the scattering rate $\Gamma = 11$ meV$/\hbar$ [22].

3. Dispersion relation

We first investigate the dispersion relation (namely, the ω–k_ρ diagram) of a dielectric/graphene/dielectric structure. The permittivities of the upper dielectric region and the lower one are denoted as ε_1 and ε_2, respectively. The horizontal wave number (propagation constant) is denoted as k_ρ, and the vertical components in the two regions are k_{iz} $(i = 1,2)$, where $k_i^2 = k_\rho^2 + k_{iz}^2$. According to the surface wave condition [27], the dispersion relation for a transverse-magnetic (TM) surface wave mode is implicitly expressed as

$$\frac{\omega\varepsilon_1 k_{2z}}{(\omega\varepsilon_2 - \sigma k_{2z})k_{1z}} + 1 = 0. \tag{4}$$

If $\varepsilon_1 = \varepsilon_2 = \varepsilon$, k_ρ can be explicitly solved as:

$$k_\rho = \sqrt{k^2 - \left(\frac{2\omega\varepsilon}{\sigma}\right)^2}. \tag{5}$$

In comparison, we also list the dispersion relation of a nobel metal (dielectric/metal structure) [28]

$$k_\rho = \frac{\omega}{c}\sqrt{\frac{\varepsilon_{1r}\varepsilon_{2r}}{\varepsilon_{1r} + \varepsilon_{2r}}}. \tag{6}$$

where ε_{1r} and ε_{2r} are the corresponding relative permittivities or dielectric constants, and ε_{2r} should be interpreted as the dielectric constant of the bulk metal.

As shown in Eq. (6), metallic plasmonics supported at a dielectric/metal structure has an obvious resonant condition $\varepsilon_{1r} + \varepsilon_{2r}(\omega) \approx 0$. Different from metallic plasmonics, graphene plasmonics does not have such “resonance condition” at a specific frequency point, as shown in Eqs. (4) and (5). However, within a broadband frequency range, the momentum matching condition $k_\rho^{inc} = k_\rho$ could be satisfied due to the infinite spatial spectrum span of a dipole source. Therefore, graphene plasmonics affects photon decay rate of an emitter in a different manner compared to metallic plasmonics. To show this, two structures involving graphene and metal (gold) are studied, as illustrated in Figs. 2(a)–2(b). In the following analysis, the surface conductivity of graphene is calculated from Eq. (3), and the dielectric constant of gold is taken from the Brendel-Bormann model in [29]. For the structure in Fig. 2(a), we set the frequency band from the infrared to visible light regime, with vacuum wavelengths from $0.5\,\mu$m to $5\,\mu$m. For the structure in Fig. 2(b), we set it to be in the visible light regime, with vacuum wavelengths from $0.4\,\mu$m to $0.8\,\mu$m. The dispersion relations are shown in Figs. 2(c)–2(d). In Fig. 2(c), the dispersion peak of graphene does not vary with respect to the dielectric material, where the black solid line indicates the turning position where the permittivity of the graphene varies from negative to positive (from plasmonic to normal material). Moreover, there is no obvious resonance peaks in the infrared regime. In Fig. 2(d), we can see that the dielectric material affects the dispersion of metal, where the black solid lines indicate the dispersion peaks. A z-oriented dipole is put 10 nm above the interface and the photon decay rates are recorded in Figs.

#225356 - $15.00 USD Received 21 Oct 2014; revised 19 Dec 2014; accepted 19 Dec 2014; published 30 Jan 2015

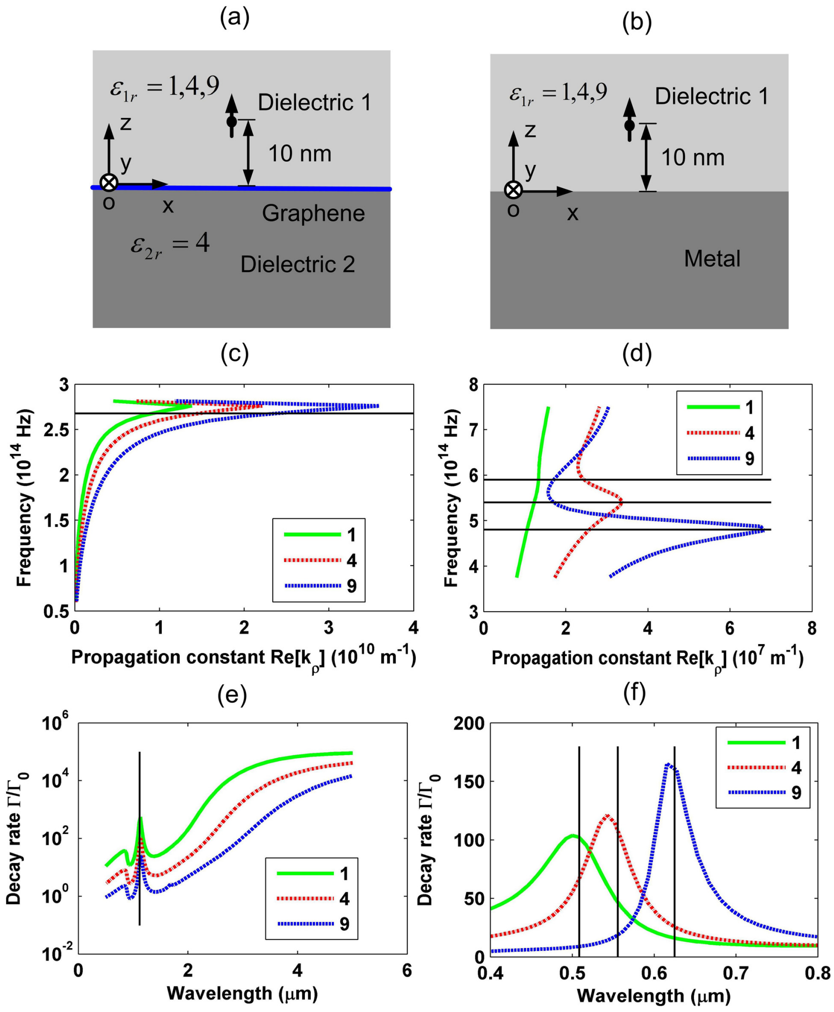

Fig. 2. (a) A dielectric/graphene/dielectric structure. (b) A dielectric/metal (gold) structure. (c) The dispersion curves of the graphene structure in the infrared and visible light regime. (d) The dispersion curves of the metal structure in the visible light regime. (e) The photon decay rate of the graphene structure with a *z*-oriented dipole 10 nm above the interface. (f) The photon decay rate of the metal structure with a *z*-oriented dipole 10 nm above the interface.

#225356 - \$15.00 USD Received 21 Oct 2014; revised 19 Dec 2014; accepted 19 Dec 2014; published 30 Jan 2015

2(e)–2(f). In Fig. 2(e), we observe the enhanced decay rate in the infrared regime with a broad range (the pseudo-peaks denoted by the black solid line indicate zero permittivity of graphene). In comparison, the decay rate enhancement in Fig. 2(f) strictly follows the resonance condition revealed by the dispersion curves. Moreover, we can see that in a planar multilayered structure, graphene plasmonics could achieve a very large photon decay rate compared to metallic plasmonics.

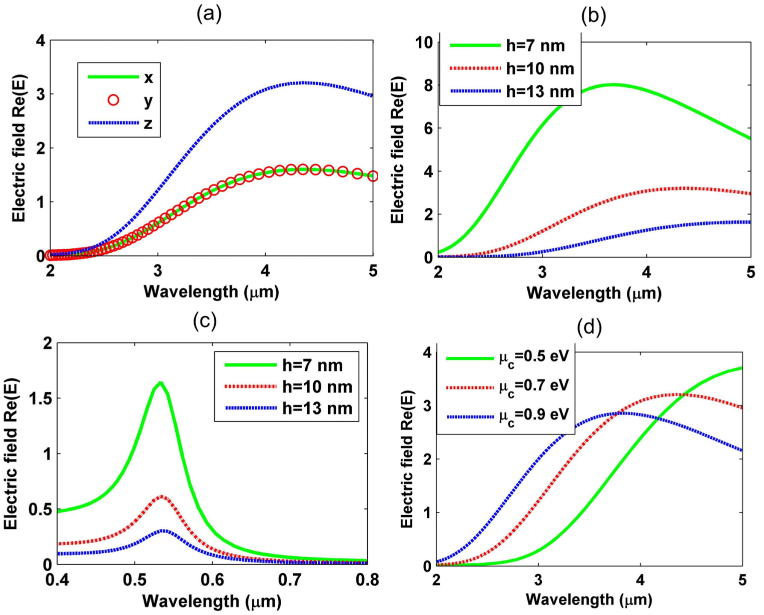

Fig. 3. (a) Polarization effect of a dipole 10 nm above the graphene layer. (b) Position effect of a *z*-oriented dipole above the graphene layer. (c) Position effect of a *z*-oriented dipole above a metal substrate. (d) Chemical potential effect of a *z*-oriented dipole 10 nm above the graphene layer.

4. Numerical results and discussion

As is shown in the previous section, graphene plasmonics and metallic plasmonics occur in the different frequency bands. Hence, it is difficult to couple the graphene plasmonics to a normal metallic scatterer. To make such coupling possible, we carefully design a split-ring resonator with well-engineered dimensions so that it can resonate in the same frequency band as the graphene does. The split-ring resonator is embedded in the layer of ZnO. A graphene layer is introduced next to the ZnO layer and is backed by a layer of SiO_2 substrate, as shown in Fig. 1. Such a layered schematic pattern is usually required in experiments. In the following, we first consider the effect from the graphene plasmonics solely, in the absence of the metallic nano structure. Since the imaginary part of the Green's function translates to the real part of the electric field generated by a dipole source, we record the electric field for convenience, as is shown in Fig. 3. In Fig. 3(a), the polarization effect is demonstrated. Three differently-oriented dipoles are put 10 nm above the graphene layer. Compared to the horizontal ones, the *z*-oriented dipole generates stronger electric field vertical to the graphene surface and thus generates more surface charge to favor surface plasmons. Also, due to the azimuth symmetry, the *x*- and *y*-oriented dipoles have the same effects. In Fig. 3(b), the position effect is tested. Three *z*-oriented dipoles with different vertical distance to the graphene are considered. The electric field at the dipole point shows a significant position-dependent feature not only on the amplitude but also on the spectral shape. Differently, the electric field above a metal layer has a narrow band; and the resonant peak does not depend on the position of the dipole, as depicted in Fig. 3(c) where the graphene layer is removed and the SiO_2 substrate is replaced by a gold layer with the same thickness. Again, the frequency band should be set to be the visible light regime in this case to allow for metallic plasmonics. In Fig. 3(d), the influence of chemical potential on electric field is investigated. The chemical potential can be easily controlled by an external electrostatic voltage gate, which is one of the unique features of the graphene plasmonics for tunable devices. It is shown that the peak is blue-shifted as the chemical potential increases [22].

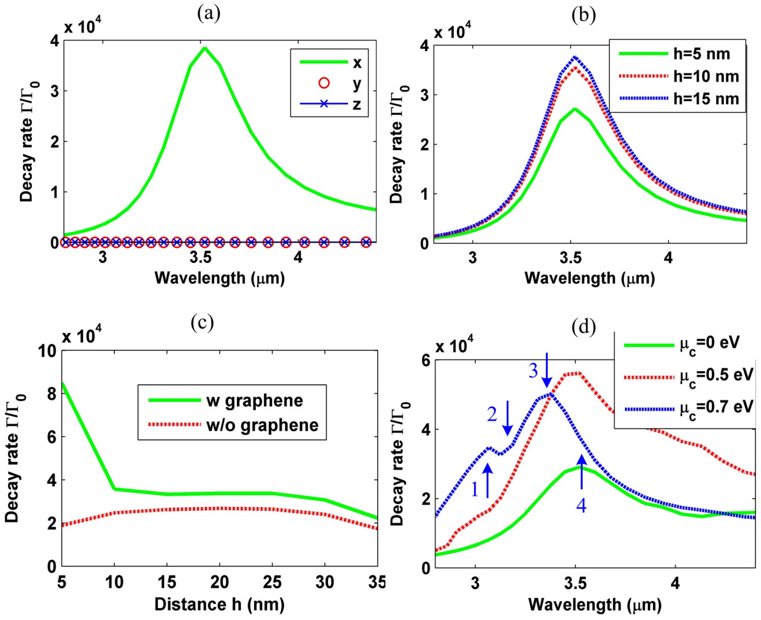

Fig. 4. (a) Polarization effect of a dipole at the center of the resonator gap without a graphene layer. (b) Position effect of a *x*-oriented dipole inside the resonator gap without a graphene layer. (c) Position effect of a *x*-oriented dipole with and without a graphene layer. (d) Chemical potential effect of a *x*-oriented dipole in the hybrid system.

Next, the split-ring resonator is incorporated into our system. Again, in order to show the response of this metallic nano-scatterer, the graphene layer is first removed. The dipole is put inside the gap of the split ring to achieve a strong confinement of the localized field. Fig. 4(a) shows the polarization effect. Apparently, this structure is polarization sensitive, and only the *x*-oriented dipole (along the arm of the resonator) couples effectively to the resonator. In Fig. 4(b), the position effect is also investigated. The dipole position affects the magnitude of the resonance peak, while leaves the peak position unchanged. This is due to the fact that the resonance frequency is determined by the dimension of the resonator and its electromagnetic environment. Finally, we consider the hybrid system with a graphene layer. The wavelength is set to be $3.38\,\mu$m and the photon decay rate of an *x*-polarized dipole is recorded along the *z* axis in Fig. 4(c). The photon decay rate inside the gap is almost symmetric with respect to the center of the structure. After introducing a graphene layer, the photon decay rate is further enhanced; and the symmetry is broken when the dipole is very close to the graphene surface. The symmetry breaking is due to the large amount of coupling (decay) channels provided by the graphene plasmonics. Hence, hybridizing the graphene with the split-ring resonator will

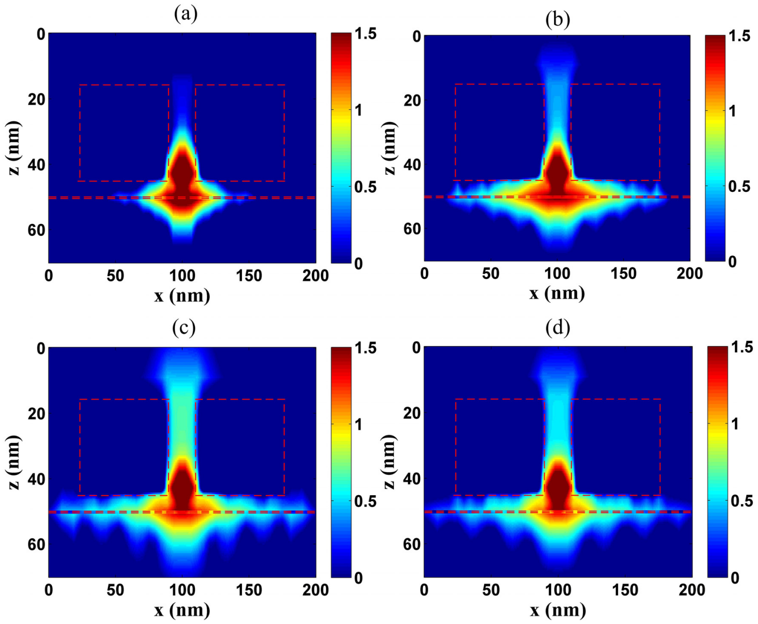

Fig. 5. (a) Near field distribution at wavelength 1 of Fig. 4(d) (shorter-wavelength peak). (b) Near field distribution at wavelength 2 of Fig. 4(d) (dip). (c) Near field distribution at wavelength 3 of Fig. 4(d) (longer-wavelength peak). (d) Near field distribution at wavelength 4 of Fig. 4(d).

offer us more degrees of freedom to control the photon decay rate with the polarization and position of the emitter and particularly with the chemical potential. In Fig. 4(d) we compare the photon decay rate with $\mu_c = 0$ eV, $\mu_c = 0.5$ eV, and $\mu_c = 0.7$ eV. The dipole is inside the gap and is 7 nm above the graphene sheet. One can see that as the chemical potential increases, the photon decay rate is not only blue-shifted [25] but also splits due to a strong coupling between graphene and the metallic resonator.

Finally, Fig. 5 shows the near-field distribution of the hybrid system at different wavelengths denoted by arrows in Fig. 4(d). First, graphene plasmonic waves are excited and decay vertically away from the graphene sheet. Evanescent waves from the dipole emitter and those from the gap of split ring offers additional momentum (k_{ev}) to excite graphene plasmonics satisfying the momentum matching condition $k_{ev} \approx k_\rho^{gra}$. Second, at the top of the split-ring gap (around $z = 15$ nm), the electric field shows a maximum intensity at wavelength 3, which suggests the decay rate peak at the longer wavelength is mainly due to the split-ring resonance. Contrarily, regarding the other decay rate peak at the shorter wavelength 1, strong graphene plasmonic waves with a shorter wavelength of $2\pi/\mathrm{Re}\left(k_\rho^{gra}\right)$ penetrate into the split ring from the bottom of the gap. Third, out-of-phase coupling between metallic plasmonics and graphene plasmonics can be observed at the decay rate dip (wavelength 2) where graphene plasmonics shows a significant spatial spread along the lateral (x) directions. In-phase and out-of-phase coupling between the split ring and graphene sheet induces the interesting physical phenomenon and opens up a new degree of freedom to electrically tune the photon decay rate.

#225356 - $15.00 USD Received 21 Oct 2014; revised 19 Dec 2014; accepted 19 Dec 2014; published 30 Jan 2015

5. Conclusion

Photon decay rate of a dipole near a metallic split-ring resonator, which is embedded in a multilayered substrate incorporating a graphene layer, is investigated in this paper. The boundary element method with the kernel of multilayered medium Green's function is developed to calculate the electromagnetic response in the complicated system. The dispersion relation of graphene plasmonics and metallic plasmonics are comparatively studied. The effects of emitter position and polarization as well as chemical potential are investigated carefully. A strong coupling between the metallic resonator and graphene can be achieved by a careful design. This work is important to explore the photon decay rate near a complex nano-structure integrated in a layered substrate involving a graphene layer. The unique feature of graphene plasmonics is helpful to dynamically control the photon decay rate.

Acknowledgments

This work was supported in part by the National Natural Science Foundation of China (NSFC 61201002, 61271158, and 61425010), in part by Research Grants Council of Hong Kong (GRF 712612 and 711511), AOARD 124082 and 134140 contracted through UTAR, and Hong Kong UGC AoE/PC04/08.

#225356 - $15.00 USD Received 21 Oct 2014; revised 19 Dec 2014; accepted 19 Dec 2014; published 30 Jan 2015